Langmuir

Article

pubs.acs.org/Langmuir

Redox Switching of Heteropolyanions Entrapped in Polypyrrole Films Investigated by ac Electrogravimetry

L. To Thi Kim,[†,‡] C. Debiemme-Chouvy,[†,‡] C. Gabrielli,[†,‡] and H. Perrot*[,†,‡]

[†]CNRS-UPR 15, LISE, 4, place Jussieu, 75252 Paris cedex 05, France

[‡]University P. and M. Curie, LISE, 4, place Jussieu, 75252 Paris cedex 05, France

ABSTRACT: In this work, the global kinetics and the exchange of protons and free solvent at the film/electrolyte interface were investigated when a PPy film doped with HPA (heteropolyanions) is polarized. The ionic and electronic transfers for the PPy-HPA system are fast because the determined values of the resistances are relatively low (a few ohms). Depending on the applied potential, the global kinetics is controlled by both the ionic and electronic transfers. The transport effects were neglected here because the prepared films were very thin. Protons play an important role in charge compensation whatever the imposed potential on the PPy-HPA film. This phenomenon results from the acidic−basic properties of the $SiMo_{12}O_{40}^{4-}$ reduced species. A small quantity of water was also shown to be involved in the film reaction process.

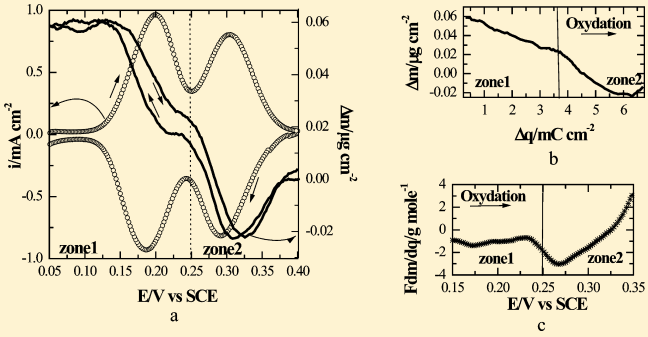

1. INTRODUCTION

Polyoxometalates such as heteropolyacids of the Keggin type, general formula $H_nXM_{12}O_{40}$ $(XM_{12}O_{40})^{n-}$, and their salts have been studied since the 1980s because of their attractive properties: nanometric size, large molar mass, proton and electron storage and transfer possibilities, and thermal stability. Their main applications are in the domain of catalysis, electrochromic systems, and cation detectors.[1] As examples, molybdenum heteropolyacids are used as catalysts for important industrial reactions: hydrodesulfurization, olefin epoxidation, alkylation,[2] and chlorate reduction.[3] These heteropolyanions (HPAs) can be immobilized in conducting polymers to form inorganic−organic hybrid materials with attractive properties such as flexibility, thermal stability, and ohmic resistance. Among possible conducting polymers, polyaniline,[4] polythiophene,[5] polypyrrole,[1,3,6] and polypyrrole films were chosen as a conducting matrix to immobilize silicomolybdate (X = Si, M = Mo, n = 4) HPAs. Polypyrrole films (PPy) were obtained by electrochemical synthesis. During polypyrrole electrogeneration, HPAs were incorporated into the polymer structure as counterions. All of the Mo atoms have a +VI degree of oxidation in the most oxidized form of HPAs. In an acid electrolyte (i.e., pH values between 0 and 1), reduced HPAs are protonated and some Mo atoms pass into the +V oxidation state (HPA blue). The involved reactions are reversible and occur at two different potentials:

$$SiMo^{VI}{}_{12}O_{40}{}^{4-} + 2H^+ + 2e^- \rightleftarrows H_2SiMo^{VI}{}_{10}Mo^{V}{}_{2}O_{40}{}^{4-} \quad (1)$$

$$H_2SiMo^{VI}{}_{10}Mo^{V}{}_{2}O_{40}{}^{4-} + 2H^+ + 2e^- \rightleftarrows H_4SiMo^{VI}{}_{8}Mo^{V}{}_{4}O_{40}{}^{4-} \quad (2)$$

The PPy-HPA composite structure has been studied in our laboratory. Different surface analysis techniques were used, such as XPS and RBS[7,8] (Rutherford back scattering), and thus HPA incorporation into the polypyrrole matrix was confirmed. By cyclic voltammetry, the electrochemical response of the PPy-HPA film in an acidic medium was examined. For a potential range between 0.05 and 0.4 V versus SCE, polypyrrole is totally oxidized and plays only the role of conducting matrix and HPAs are the only redox species involved in the redox switching of the PPy-HPA film.[8] The two redox responses of HPA are observed at around 0.2 and 0.3 V versus SCE. A more sophisticated technique, called ac electrogravimetry, was carried out to check that the electron transfer was counterbalanced by cation transfer for all of the potential values[9] in sulfuric and potassium media.

The aim of this work was to carry out a more systematic investigation of the redox switching of PPy-HPA films in aqueous perchlorate solution by ac electrogravimetry within the whole domain of electroactivity of these films and then to describe carefully the exchange process of electrons, protons/cations, and free solvent at the different interfaces. For that purpose, a more sophisticated model was developed and tested in comparison with the previous one based on a compact film and only ionic transfer.

2. THEORY

In this part, a summary of the model based on porous electroactive films, used in the following text, is given. In fact, to reach the entrapped HPAs the charged species have to cross PPy through pores. A model based on a transmission line has

Received: May 24, 2012
Revised: August 21, 2012
Published: August 29, 2012

 © 2012 American Chemical Society dx.doi.org/10.1021/la302115f | *Langmuir* 2012, 28, 13746−13757

been developed by De Levie.[10−12] This simple model considers a cylindrical pore with length L and radius r_0. The pore wall is supposed to react with the electrolyte. The behavior of this pore called active differs from that of pores called passive, where reactions occur only at the pore end. The current flowing through the pore provokes an ohmic drop related to the resistivity of the electrolyte in the pore. Therefore, as part of the current passes through the pore wall, the local current varies with the pore depth x. This is the cause of the particular behavior of porous electrodes: on one hand, potential and current distributions are observed in the pore, and on the other hand, an axial distribution of the concentration of the active species is also observed if reactions occur on the pore wall.

By assuming that the axial concentration gradient is negligible (i.e., the species concentration $c(x)$ is a constant along the pore length), De Levie[10−12] has calculated the pore impedance, $Z_P(\omega)$, in the form

$$Z_P(\omega) = \sqrt{\rho Z_0(\omega)}\coth\left[L\sqrt{\frac{\rho}{Z_0(\omega)}}\right] \tag{3}$$

where ω is the pulsation ($\omega = 2\pi f$), ρ is the pore resistivity, and $Z_0(\omega)$ is the impedance located on the electrolyte/pore wall that will be given below.

In the low-frequency range ($\omega \to 0$), $Z_0 \gg \rho$, then $\coth[L(\rho/Z_0(\omega))^{1/2}] = (1/(L(\rho/Z_0(\omega))^{1/2})) + ((L(\rho/Z_0(\omega))^{1/2})/3)$ and

$$Z_P(\omega) = \frac{Z_0(\omega)}{L} + \frac{\rho L}{3} \tag{4}$$

Hence, the impedance of a cylindrical pore is equal to that of a flat electrode with the same area as the developed pore surface but with a shift of the real part equal to a third of the ohmic drop of the pore with unit area $\Omega = \rho L$.

In the high-frequency range ($\omega \to \infty$), $Z_0 \ll \rho$, then $\coth[L(\rho/Z_0(\omega))^{1/2}] = 1$ and therefore

$$Z_p(\omega) = \sqrt{\rho Z_0(\omega)} \tag{5}$$

does not depend on the pore length. It is called the impedance of a semi-infinite cylindrical pore.

Therefore, impedance measurements allow the pore texture of a porous electrode to be characterized by its equivalent pore radius, r_0, and pore length, L.

On the pore wall, species transfer occurs at the film/electrolyte interface.[13,14] Generally speaking, the flux of species i (a, anion; c, cation; s, solvent), J_i, is considered to be positive if the species is expelled from the film

$$J_i > 0 \text{ for } x > 0 \tag{6}$$

where x represents the distance from the film surface toward the electrolyte.

The doping mechanism of an electroactive film by a cation can be described by the following reaction

$$\langle P\rangle + e^- + c^+ \underset{k'_c}{\overset{k_c}{\rightleftarrows}} \langle P, c^+\rangle \tag{7}$$

where $\langle P\rangle$ is a free electroactive site on the film and $\langle P, c^+\rangle$ represents the cations inserted into the film at specific sites.

By using the laws of the heterogeneous kinetics and reaction 7, we can write the flux J_c of the cations at the film/solution interface as

$$J_c(d_f) = -d_f\frac{dC_c}{dt} = k'_c(C_c - C_{c_{min}}) - k_c(C_{c_{max}} - C_c)C_{c_{sol}} \tag{8}$$

where d_f is the film thickness.

By using the Hillman solvation model,[15] we can use the same relationship for the solvent flux

$$J_s(d_f) = -d_f\frac{dC_s}{dt} = k'_s(C_s - C_{s_{min}}) - k_s(C_{s_{max}} - C_s) \tag{9}$$

where C_i is the concentration of species i in the film, $C_{i_{sol}}$ is the concentration of species i in the solution by assuming that the diffusion of ions in solution does not limit the global kinetics; the term $[C_{i_{max}} - C_i]$ is the concentration of free sites for species i at time t, with $C_{i_{max}}$ being the maximum concentration of the free sites in the film for species i; and $[C_i - C_{i_{min}}]$ is the concentration of species i in the film bulk at time t, with $C_{i_{min}}$ being the minimum concentration of species i in the film.

Finally, the kinetic constants depend on the potential in the form

$$k'_i = k'_{i_0}e^{[b'_i(E-E_i^\circ)]} \quad k_i = k_{i_o}e^{[b_i(E-E_i^0)]} \tag{10}$$

where E is the potential; E_i° is the apparent normal potential; $(E - E_i^\circ)$ is the overvoltage; and k_{i_0}, k'_{i_0}, b_{i_0}, and b'_{i_0} are constants.

By considering that the electrolyte contains only two types of monovalent cations and by using the Faraday law, the current density, j_F, at the film/electrolyte interface ($x = d_f$) is

$$J_{c_1}(d_f) + J_{c_2}(d_f) = \frac{I_F}{F} \tag{11}$$

All of the cations can be considered in our case, but only monovalent ions were tested here. It should be noticed that, in the case of divalent ions, the model is also valid.

On the contrary, at the electrode/film interface ($x = 0$), where only electrons are exchanged, the flux of ions and solvent is

$$J_{c_1} = J_{c_2} = J_s = 0 \tag{12}$$

Now, the insertion laws can be determined. In the dynamic regime, under the effect of a potential sinusoidal perturbation with low amplitude, ΔE, imposed on the electrode/film/electrolyte system, sinusoidal fluctuations of concentration, ΔC_i, and flux, ΔJ_i, are observed, such as

$$\Delta J_i = -d_f\frac{dC_i}{dt} = -j\omega d_f\Delta C_i \tag{13}$$

However, the expression of the global insertion/expulsion flux, ΔJ_i, which depends on the concentration and potential perturbations at the polymer/electrolyte interface ($x = d_f$) is, considering first-order development under linear conditions,

$$\Delta J_i = \left(\frac{\partial J_i}{\partial C_i}\right)_E \Delta C_i + \left(\frac{\partial J_i}{\partial E}\right)_{C_i}\Delta E = K_i\Delta C_i(d_f) + G_i\Delta E \tag{14}$$

where

$$K_i = \left(\frac{\partial J_i}{\partial C_i}\right)_E = k'_i + k_iC_{i_{sol}} \tag{15}$$

dx.doi.org/10.1021/la302115f | Langmuir 2012, 28, 13746−13757

$$G_i = \left(\frac{\partial J_i}{\partial E}\right)_{C_i} = [b_i' k_i'(C_i - C_{i_{min}}) - b_i k_i (C_{i_{max}} - C_i) C_{i_{sol}}] \quad (16)$$

where K_i is the time constant of the global transfer kinetics of species i and G_i is the inverse of the transfer resistance of the species at the film/solution interface (where i is the cation c or solvent s). From eqs 13 and 14, the insertion law can be written in the form

$$\frac{\Delta C_i}{\Delta E}(\omega) = \frac{-G_i}{j\omega d_f + K_i} \quad (17)$$

where $G_i > 0$ for the cations. This gives the concentration response of species i to a potential perturbation.

$$\text{local electrochemical impedance} = \frac{\Delta E}{\Delta I}(\omega)$$

In the dynamic regime, the perturbation ΔE leads to a variation in the charge of the film by considering that two cations, in our case, are involved in the charge compensation process at the pore wall. In addition, the faradaic current density is such that $\Delta I_F = j\omega\Delta q$, and this relation is valid under potential sine wave modulation. By dividing by ΔE and assuming that $\Delta q = -Fd_f(\Delta C_{c_1} + \Delta C_{c_2})$, the faradaic admittance is calculated when two monovalent cations are involved in the charge compensation process:

$$\frac{\Delta I_F}{\Delta E} = -j\omega F d_f \left(\frac{\Delta C_{c_1}}{\Delta E} + \frac{\Delta C_{c_2}}{\Delta E}\right) \quad (18)$$

Therefore, by using eq 17, the faradaic impedance relative to the global ionic transfer of the electroactive film for two cations (c_1 and c_2) involved in the charge compensation is

$$Z_F(\omega) = \frac{\Delta E}{\Delta I_F}(\omega) = \frac{1}{j\omega d_f F\left[\frac{G_{c_1}}{j\omega d_f + K_{c_1}} + \frac{G_{c_2}}{j\omega d_f + K_{c_2}}\right]} \quad (19)$$

2.1. Electrochemical Impedance of a Porous Electroactive Film. To simplify the model, the electroactive film is supposed to be constituted of cylindrical pores full of electrolyte where the insertion/expulsion reactions occur on the wall.

The impedance of the electrolyte/pore wall, Z_0, corresponds to the faradaic impedance related to the global ionic transfer, Z_F, in parallel with a double-layer capacity C_d at the pore wall/electrolyte interface. Then, Z_0 can be expressed as

$$Z_0(\omega) = \frac{1}{j\omega C_d + \frac{1}{Z_F}} \quad (20)$$

The global electrochemical impedance, $Z(\omega)$, of the porous electroactive film that is experimentally measured is the sum of the impedance related to the electronic transfer at the electrode/film interface, Z_e, and the impedance of the pore, Z_p, calculated with eq 3

$$Z(\omega) = Z_e + Z_P = \frac{1}{\frac{1}{R_e} + j\omega C_e} + \sqrt{\rho Z_0(\omega)}\ \coth\left[L\sqrt{\frac{\rho}{Z_0(\omega)}}\right] \quad (21)$$

where R_e and C_e are the electronic transfer resistance and capacity at the electrode/film interface. Here, a basic equivalent circuit was used to characterize this electronic transfer.

2.2. Charge/Potential Transfer Function. The charge/potential transfer function gives information on the ionic transfer. From eq 20, we obtain

$$\frac{\Delta q}{\Delta E}(\omega) = \frac{1}{j\omega}\frac{1}{Z_0} = C_d + \frac{1}{j\omega Z_F} \quad (22)$$

$$\text{electrogravimetric transfer function} = \frac{\Delta m}{\Delta E}(\omega)$$

The ΔE perturbation leads to a change in the charge compensation related to the species going in and out (cation, anion, and solvent) of the film. It should be mentioned that the solvent cannot play a direct role in the charge compensation process but plays an indirect role because of electrosmotic effects, electrochemical drag, or steric exclusions. This leads to a mass variation Δm related to each concentration change ΔC_i, and by dividing this relation by ΔE, the function $((\Delta m)/(\Delta E))(\omega)$ becomes

$$\frac{\Delta m}{\Delta E}(\omega) = d_f\left[m_c\frac{\Delta C_c}{\Delta E} + m_a\frac{\Delta C_a}{\Delta E} + m_s\frac{\Delta C_s}{\Delta E}\right] \quad (23)$$

where m_c, m_a, and m_s are the atomic weights for each involved species.

In eq 17, the global electrogravimetric transfer function per surface unit, taking into account two types of cations and solvent, is

$$\frac{\Delta m}{\Delta E}(\omega) = -d_f\left(m_{c_1}\frac{G_{c_1}}{j\omega d_f + K_{c_1}} + m_{c_2}\frac{G_{c_2}}{j\omega d_f + K_{c_2}} + m_s\frac{G_s}{j\omega d_f + K_s}\right) \quad (24)$$

The experimental data were fitted to the model of the porous electroactive film described above to obtain the kinetic parameters. The three transfer functions—electrochemical impedance, charge/potential transfer, and electrogravimetric transfer—were used separately.

The fitting procedure applied to the electrochemical impedance allows the parameters relative to the electronic and ionic transfers and the porosity of the electroactive film to be extracted.

The validity of the model and of the different associated parameters obtained is checked by comparison with other models, for example, on the basis of only ionic transfer. In this last case, the intermediate frequencies of the electrochemical impedance are completely neglected, and visually, it appears that the model is not adapted. Moreover, a quantitative criteria based on a correlation variable is calculated and can justify the good quality of the fittings.

The charge/potential transfer function gives information on the ionic transfer and the electrogravimetric transfer function for the atomic masses of the involved species in the charge compensation process.

Au coated with PPy-HPA film electrodes was first studied in acidic medium ($HClO_4$ 0.5M) and then in $KClO_4$ solutions at various pH values adjusted by adding perchloric acid.

3. MATERIALS AND METHODS

PPy-HPA films were electrodeposited on one of the gold electrodes of an electrochemical quartz crystal microbalance (EQCM) from an aqueous solution containing 2×10^{-2} M α-$H_4SiMo_{12}O_{40}$ (α-silicomolybdate acid obtained from Aldrich) + 10^{-2} M pyrrole (previously distilled). These films were synthetized in galvanostatic mode ($I = 0.015$ mA) for 1250 s to obtain a 150 nm film thickness. The working electrode used here is one of the gold electrode deposited on one face of the quartz resonator, with a surface area of 0.2 cm^2, in contact with the electrolyte. It was estimated via

dx.doi.org/10.1021/la302115f | Langmuir 2012, 28, 13746−13757

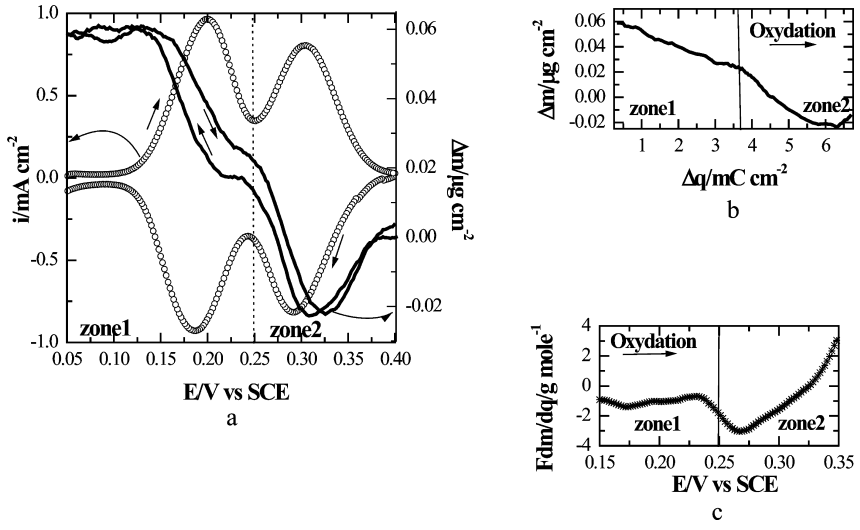

Figure 1. i–E, Δm–E (a), Δm–Δq (b), and $F\,dm/dq$–E (c) curves of a PPy-HPA film in 0.5 M $HClO_4$ with respect to potentials between 0.05 and 0.4 V vs SCE for a 20 mV s^{-1} scan rate.

its cross section observed by scanning electrochemical microscopy. PPy-HPA films were conditioned for 30 min in the studied medium before measurements of the cyclic electrogravimetry and ac electrogravimetry were begun.

ac electrogravimetric measurements were carried out by using a four-channel-frequency response analyzer (Solartron 1254 TFA) and a laboratory-made potentiostat and EQCM. Details of the experimental equipment are given elsewhere.[16−18]

4. RESULTS

4.1. PPy-HPA Film Behavior in 0.5 M $HClO_4$. Electrogravimetric measurements by means of potential scanning or low-amplitude sinusoidal perturbation of the potential were carried out at various imposed potentials on PPy-HPA films in 0.5 M $HClO_4$ solution (pH 0.3).

4.1.1. Cyclic Electrogravimetry. PPy-HPA films were first studied by cyclic electrogravimetry. Figure 1a shows the variations in the current and mass of the PPy-HPA film when it is reduced and reoxidized between 0.05 and 0.4 V versus SCE at a 20 mV s^{-1} scan rate in a 0.5 M $HClO_4$ solution. The current exhibits two reversible redox peaks that correspond to the two first redox systems of $SiMo_{12}O_{40}^{4-}$ (reactions 1 and 2). The area of the second (reaction 2) peak (zone 2) is slightly smaller than the area of the first (reaction 1) peak (zone 1). The increase in the film mass during the HPA reduction indicates that the charge compensation is mainly due to cation insertion. However, between 0.3 and 0.4 V versus SCE there is an inversion of the mass change. Moreover, the variation of the film mass is reversible between the HPA's reduced and reoxidized states.

The molar mass of the species that participate in the charge compensation process was also calculated roughly from the slope of the Δm–Δq curve (Figure 1b): for the second zone of potential, a mean mass of about 1 g mol^{-1} is obtained, which obviously corresponds to proton participation. For the first zone of potential, a mass of about 2 g mol^{-1} corresponds to the participation of several species as exchanges of protons (M = 1 g mol^{-1}) and solvent (M = 18 g mol^{-1}) during film oxidation. This approach does not allow perfect discrimination to be obtained.

In a more precise way than previously, values of $F\,dm/dq$ were calculated from the current and mass using eq 25. This allows the nature of the species participating in the charge compensation process to be estimated at each potential value (Figure 1c).

$$F\frac{dm}{dq} = F\frac{dm/dt}{dq/dt} = F\frac{dm/dt}{I} \tag{25}$$

The apparent value of the atomic mass of the species is different for the two HPA redox reactions. For the first (zone 1) redox peak (0.15 to 0.25 V vs SCE), the $F\,dm/dq$ value is practically constant and equal to 1 g mol^{-1}, in absolute value, which corresponds to the mass of the proton. For the second peak (0.25−0.32 V vs SCE), $F\,dm/dq$ changes with respect to the potential and reaches a minimal value equal to −3 g mol^{-1} at 0.27 V versus SCE, which shows that the charge compensation process is due to the participation of several species (e.g., expulsion of water together with the protons). For potentials between 0.3 and 0.35 V, the $F\,dm/dq$ function varies from de − 1 to 2 g mol^{-1}, which could be interpreted by water expulsion concomitantly with proton insertion when the HPAs entrapped in the PPy film are reduced. Consequently, charge compensation seems to be essentially due to proton insertion in the whole potential domain associated with the exchange of solvent toward more anodic potentials.

4.1.2. ac Electrogravimetry. By using ac electrogravimetry, the chemical nature of the species and the kinetics of charge transfer can be obtained. At each imposed potential, the mass response, $\Delta m(\omega)$, and the current response, $\Delta I(\omega)$, of the film to a low-amplitude potential perturbation $\Delta E(\omega)$ (50 mV) were measured at various modulation frequencies between 63 kHz and 10 mHz. The various experimental and calculated transfer functions of the PPy-HPA film, with parameters obtained through a numerical fitting procedure, are given in Figure 2 at a potential of 0.295 V versus SCE. The electrochemical impedance $((\Delta E)/(\Delta I))(\omega)$ (Figure 2a) had the classical shape of the impedance of a blocking electrode with a quasi-vertical capacitive part in the low-frequency range. The fitting of the electrochemical impedance, based on eq 21, allows the parameters associated with this quantity to be estimated in the framework of the model of porous films previously described. The kinetics is related to an ionic-transfer process that counterbalances the electronic transfer. At this potential, the obtained resistance

dx.doi.org/10.1021/la302115f | Langmuir 2012, 28, 13746−13757

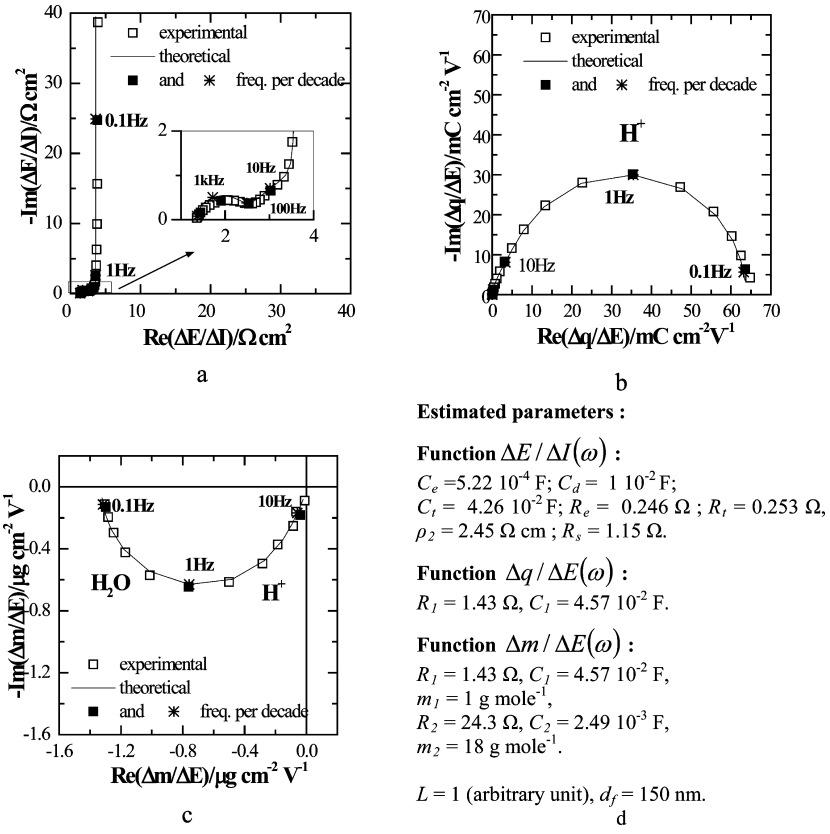

Figure 2. Experimental and calculated transfer functions (a–c) with the estimated parameters (d) at 0.295 V versus SCE for a PPy-HPA film in 0.5 M $HClO_4$.

values are practically equal for the two types of ionic (R_t = 0.25 Ω) and electronic (R_e = 0.25 Ω) transfers. This demonstrates that the exchange kinetics is controlled by both the ionic and electronic transfer. In addition, the value of the pore resistivity, equal to 2.4 Ω cm, was also estimated from the experimental electrochemical impedance. It is noticeable that a 45° slope was observed at mid frequencies (between 100 and 10 Hz) on the electrochemical impedance diagram (Figure 2a). This is related to the potential distribution imposed by the ohmic drop due to the finite conductivity of the electrolyte in the pore of the film. It is also noticeable that this diagram shows that electronic transfer occurs in the high-frequency range, between 63 and 1 kHz, and that ionic transfer occurs in the low-frequency range at the pore wall surface with a potential distribution.

The diagram of the calculated transfer function, $(\Delta q)/(\Delta E)(\omega)$, obtained from the experimental $Z = (\Delta E)/(\Delta I)(\omega)$ by using $(\Delta q)/(\Delta E)(\omega) = (1)/(j\omega(Z - R_s)$, where R_s is the solution resistance, exhibits only one loop (Figure 2b). This loop corresponds to only one charged species that participate in the charge compensation. The fitting procedure allows the values of the ionic transfer resistance, equal to 1.43 Ω, and the insertion capacity, equal to 4.57×10^{-2} F, to be extracted.

In the diagram of the transfer function, $((\Delta m)/(\Delta E))(\omega)$ (Figure 2c), a half-circular loop located in the third quadrant corresponds to cations, both cations and free solvent, and expulsion/insertion when the HPAs are oxidized/reduced. The fitting, based on eq 19, was carried out by taking into account two species (proton and free solvent). The electrogravimetric transfer function is well fitted only when the values of R_i and C_i used are estimated from the charge/potential function and for a mass equal to 1 g mol^{-1} corresponding to the proton. At last, the free-solvent contribution (M = 18 g mol^{-1}) that is indirectly associated with the charge compensation is obtained by using a transfer resistance equal to 24.3 Ω and an insertion capacity equal to 2.49×10^{-3} F. However, the two loops overlap in the diagram of the mass/potential transfer function (Figure 2c) because the insertion time constants of the two species, calculated from eq 23, are very close at this potential. Consequently, to compensate for the positive charges created by an anodic polarization imposed on the PPy-HPA film, cations are expelled, accompanied by free solvent molecules with quasi-identical kinetics (very similar values of K_i). However, data analysis demonstrates that it is free solvent and not solvent bound to H^+, such as H_3O^+, that is expelled. This result is obtained by calculating the atomic mass of each species and also is due to the high quality of the experimental set up, which allows a fair separation of the contribution of each species.

Similarly, experiments and fittings were carried out at several potentials ranging between 0.14 and 0.32 V versus SCE. Therefore, the characteristic kinetic parameters of the PPy-HPA film were analyzed with respect to the potential. Figure 3a shows the variation of the electronic transfer resistance, R_e, and of the ionic transfer resistance, R_t, estimated from the electrochemical impedance. The two minimal values of the ionic resistance are obtained at 0.2 and 0.3 V versus SCE, which correspond to the two peaks of the voltammetric curve, whereas the minimal value of the electronic resistance is obtained at 0.23 V, which corresponds to the minimum in the voltammetric curve. This means that when the two redox reactions of $SiMo_{12}O_{40}^{4-}$ (reactions 1 and 2) occur, the proton exchanges at the film/electrolyte interface are favored whereas the electronic transfer at the electrode/film interface is slightly slowed. Therefore,

dx.doi.org/10.1021/la302115f | Langmuir 2012, 28, 13746–13757

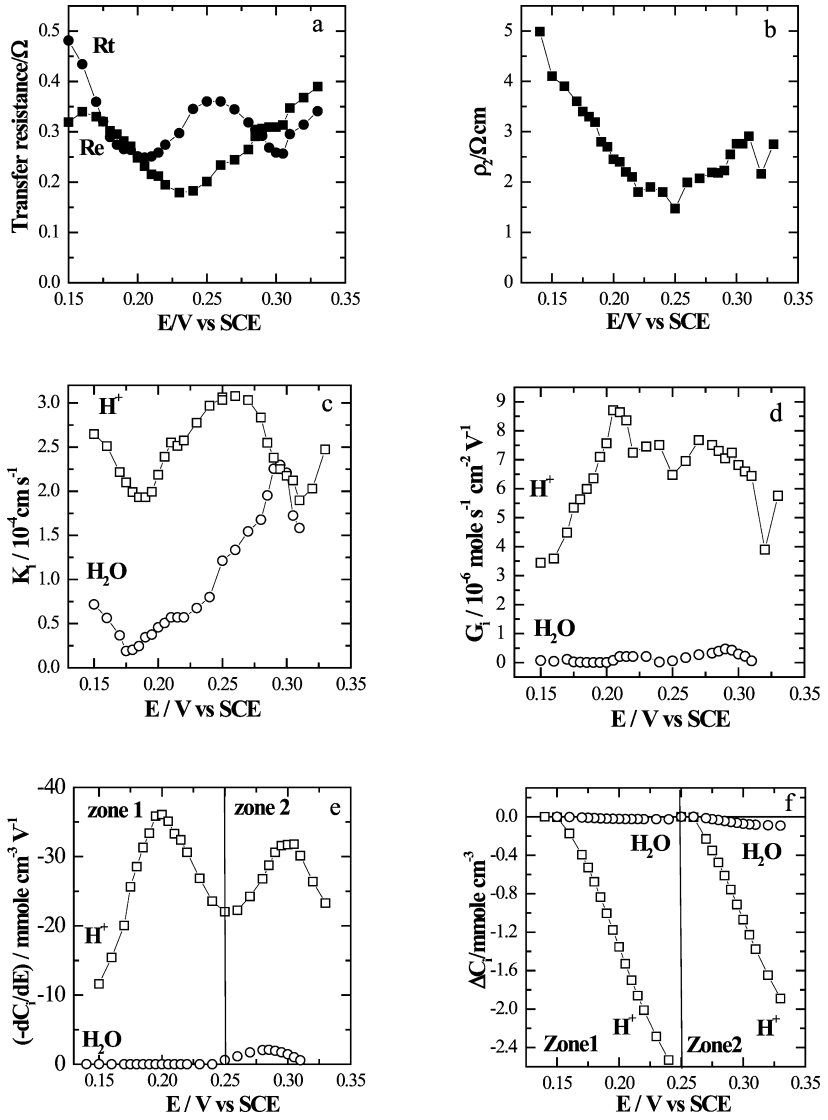

Figure 3. Variation of the transfer resistances (a) and pore resistivity (b) estimated from the electrochemical impedance with respect to the potential for a PPy-HPA film in 0.5 M $HClO_4$. Variations of K_i (c), G_i (d), dC_i/dE (e), and ΔC_i (f) with respect to the potential for a PPy- HPA film in 0.5 M $HClO_4$.

this shows that the kinetics of the charge compensation, which is rather fast, is under mixed, ionic and electronic, control. In the catalytic applications, the fast kinetics of protonic and electronic transfers are important factors that directly influence the catalytic activity of the system.[19]

Figure 3b shows an increase in the pore resistivity of the PPy-HPA film when the potential becomes more cathodic (reaction 2). This would come from the cation impoverishment in the pore as a result of cation insertion at the pore wall when the film is reduced, which would lead to a decrease in the pore conductivity. Above 0.25 V versus SCE, ρ_2 increases again, which may be due to the shrinking of the PPy matrix when the PPy-HPA film is oxidized.[20,21]

The variations of K_i, G_i, dC_i/dE, and ΔC_i with respect to the potential are given in Figure 3. To calculate these quantities, the following relationships were used:

$$K_i = \frac{d_f}{R_i C_i} \quad G_i = \frac{1}{F R_i}$$

The quantity dC_i/dE, which is the derivative of the concentrations with respect to the imposed potential for each species, can be calculated by considering the low-frequency limit of $(\Delta C_i)/(\Delta E)(\omega)$, then

$$\frac{\Delta C_i}{\Delta E}(\omega) = \frac{-G_i}{j\omega d_f + K_i} \rightarrow \frac{\Delta C_i}{\Delta E}(0) = -\frac{G_i}{K_i}$$

and ΔC_i was obtained by integrating dC_i/dE with respect to the potential.

Figure 3c shows that the proton insertion is slower for the two redox reactions of $SiMo_{12}O_{40}^{4-}$ as the value of the time constant K_i reaches two minimum values at potentials of 0.18 and 0.29 V versus SCE. However, the kinetics of the proton insertion is always faster than the free-solvent kinetics whatever the potential imposed on the film except at potentials between 0.29 and 0.3 V versus SCE where the kinetics of the two species are very close. Because the value of G_i for the proton is inversely proportional to the protonic transfer resistance, R_t, it is normal that the maximum values were found at potentials equal to 0.3 and 0.2 V versus SCE where R_t is a minimum. The

dx.doi.org/10.1021/la302115f | Langmuir 2012, 28, 13746−13757

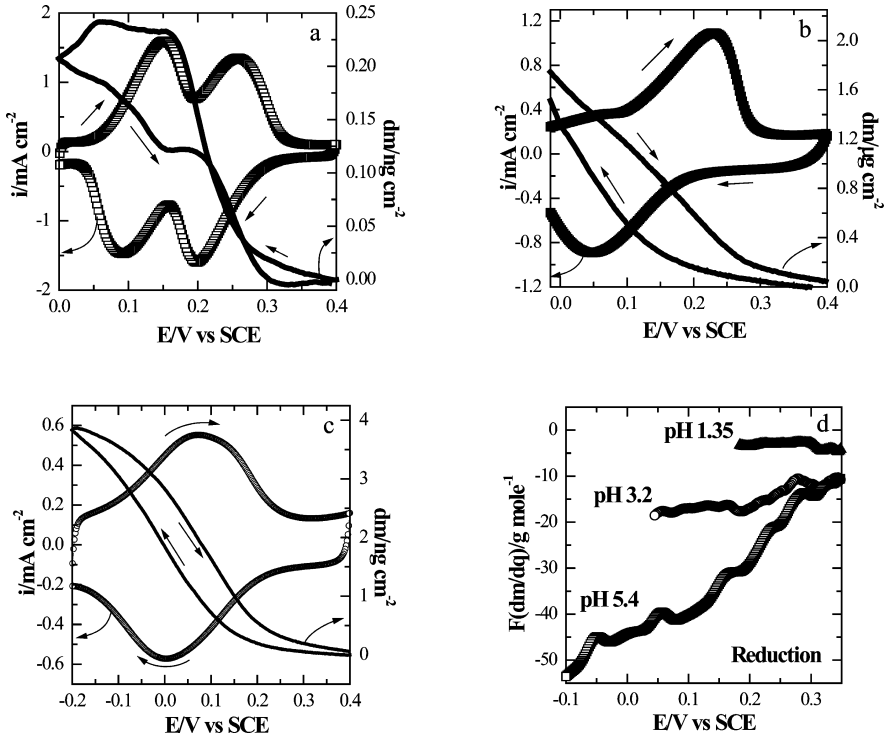

Figure 4. Cyclic voltammetric and electrogravimetric diagrams in 0.1 M $KClO_4$ at pH 1.35 (a), 3.2 (b), and 5.2 (c) and variation of $F\ dm/dq$ with respect to the potential at a 20 mV/s scan rate (d).

parameter G for the protons is much greater than the value for the solvent.

Figure 3e shows that the evolution of dC_i/dE for the protons is practically identical to the change in current measured by cyclic voltammetry when the film is reduced or oxidized. This means that the charge compensation of the film is primarily due to proton participation but is also accompanied by a slight water transfer in the same direction in each potential zone. Nevertheless, the role of the solvent is more important in the second zone whereas the role of the protons is slightly more important in the first zone. The change in the species concentrations, obtained by integrating the dC_i/dE curves in Figure 3e, describes the insertion/expulsion law of the species with respect to the potential. When the change in the concentration of the two species is considered (Figure 3f), the solvent contributes 1% in the first zone and about 5% in the second zone with respect to the total flux of exchanged matter during the reaction. The exchange of solvent between the two reduced and oxidized states during the second redox reaction of the HPAs is 4 times larger than the exchange related to the first reaction at more cathodic potentials. This result is in agreement with the molar mass calculated from cyclic voltammetry where the mass equals 1 g $mole^{-1}$ and then 2 g mol^{-1} depending on the considered potential zone. It is noticeable that water is going in the opposite direction than protons above 0.31 V, where $dC_i/dt < 0$, in agreement with the $F\ dm/dq$ function calculated earlier. This effect can be due steric exclusions or thermodynamic considerations. The evolution of the electrolyte resistivity in the film pores can be explained by the change in the quantities of species in the pores of the film. When the film is oxidized, the pore resistivity decreases in the first zone. This is due mainly to an important quantity of protons (2.53 mmol cm^{-3}) released from the film. For the second zone, a lower proton quantity (1.89 mmol cm^{-3}) is obtained whereas a more important quantity of solvent (0.091 mmol cm^{-3}) is expelled that induces a lower change in resistivity.

The proton movement is due to the acidic−basic properties of the reduced species of $SiMo_{12}O_{40}^{4-}$. When the reduction occurs, the HPA basicity increases and consequently the HPAs have a tendency to become protonated (eqs 1 and 2). The low quantity of detected water can be due to the microporous structure of the PPy matrix, which is permeable to water. It can be assumed that water can be exchanged at the pore wall of the polypyrrole matrix or that water enters the pores when protons are entering the polymer at the pore wall as species are weighted as soon as they enter the porous structure. This is in agreement with the work of Otero et al.,[22] who have shown that the PPy film is more and more hydrated when it is oxidized.

4.2. pH Influence on the PPy-HPA Film Redox Properties. Because the electroactivity of the HPAs is pH-dependent, this point has been tested by cyclic electrogravimetry and ac electrogravimetry in $KClO_4$ solutions at various pH values. In the presence of cations other than protons, we can expect some competition in the charge compensation process when $SiMo_{12}O_{40}^{4-}$ is electrochemically reduced because protons play a preferential role with respect to the HPA acidic−basic properties.

The PPy-HPA redox properties were investigated first by cyclic electrogravimetry and then by ac electrogravimetry in 0.5 M $KClO_4$ solutions at pH 1.32 and 3.5, adjusted by adding a quantity of $HClO_4$, and 5.2. The studied films were 200 nm thick.

4.2.1. Cyclic Electrogravimetry. As for a 0.5 M $HClO_4$ solution that has a pH equal to 0.3, the more acidic $KClO_4$ solution (pH 1.35) exhibits two redox peaks whereas for the less acidic $KClO_4$ solutions (pH 3.2 and 5.2) only one redox peak appears in the tested potential range (Figure 4a−c). Concerning the mass−potential curve, the shape simplifies when the pH

dx.doi.org/10.1021/la302115f | *Langmuir* 2012, 28, 13746−13757

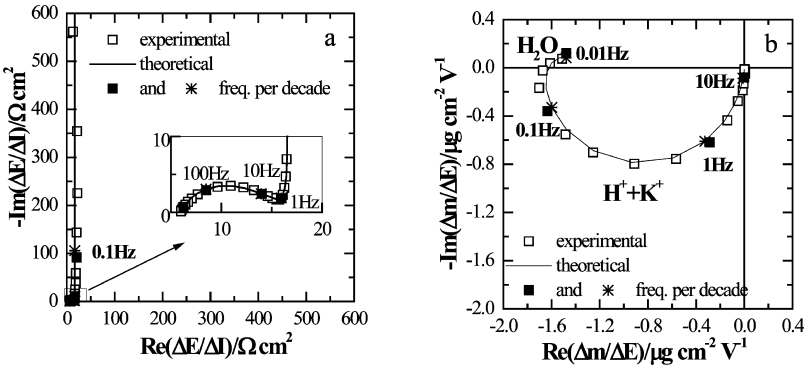

Figure 5. Experimental and theoretical transfer functions obtained at 0.25 V vs SCE for a PPy-HPA film in 0.1 M $KClO_4$ at pH 1.35. Theoretical functions were calculated with the following parameters: $C_e = 2.14 \times 10^{-4}$ F, $C_d = 2.59 \times 10^{-3}$ F, $C_t = 5.8 \times 10^{-2}$, $R_e = 3.04$ Ω; $R_t = 1.48$ Ω, $\rho_2 = 7.4$ Ω cm, $R_s = 6$ Ω for $\Delta E/\Delta I(\omega)$ (a); $K_c = 4.71 \times 10^{-5}$ cm s^{-1}, $G_c = 1.508 \times 10^{-61}$ mole s^{-1} cm^{-2} V^{-1}, $m_c = 4$ g $mole^{-1}$, $K_s = 2.51 \times 10^{-6}$ cm s^{-1}, $G_s = -4.27 \times 10^{-9}$ mole s^{-1} cm^{-2} V^{-1}, $m_s = 18$ g $mole^{-1}$ for $\Delta m/\Delta E(\omega)$ (b).

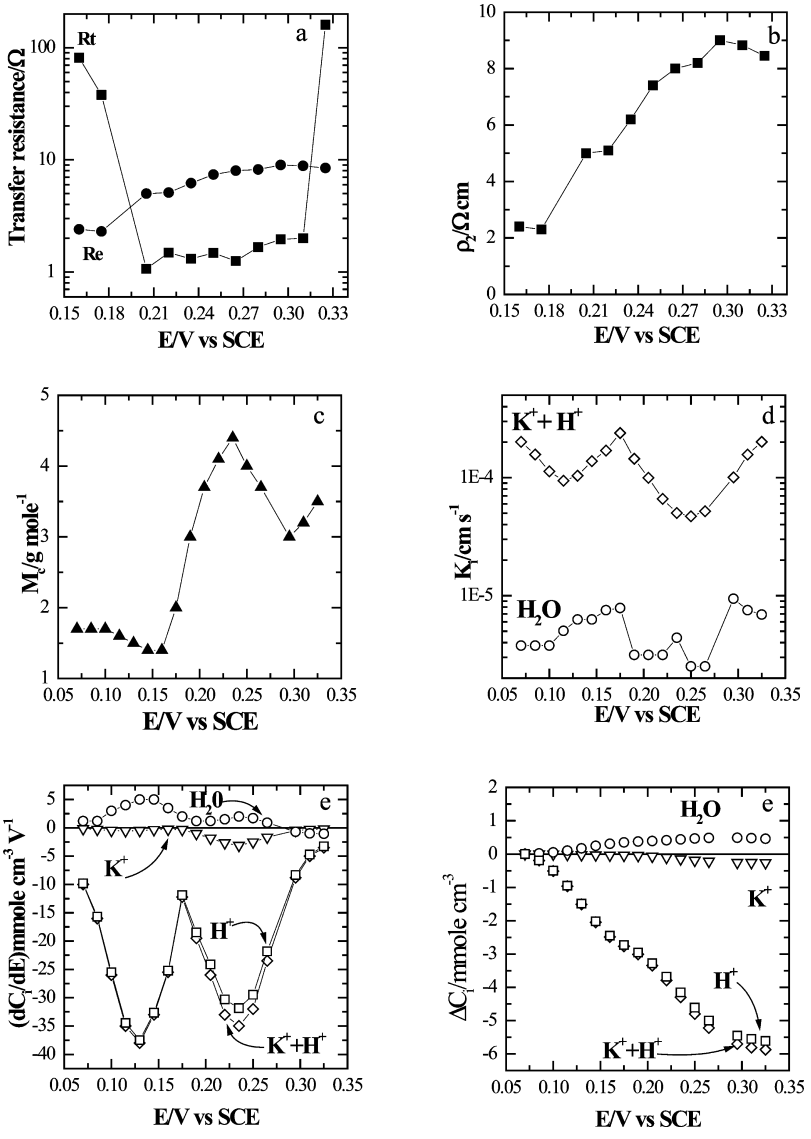

Figure 6. Variation of various calculated parameters (a–d), variation of the derivative of the insertion law (dC_i/dE) with respect to the potential (e) and variation of the species concentration ΔC_i with respect to the potential (f) for the PPy-HPA film in 0.1 M $KClO_4$ at pH 1.35.

increases. At lower pH, a very complicated shape appears. However, all pH's are characterized by the charge compensation necessary to maintain film electroneutrality involving predominantly cations as the mass increases when the imposed potential decreases to reduce the PPy-HPA film. Figure 4d shows that the apparent atomic mass of the involved cations increases from

dx.doi.org/10.1021/la302115f | *Langmuir* 2012, 28, 13746–13757

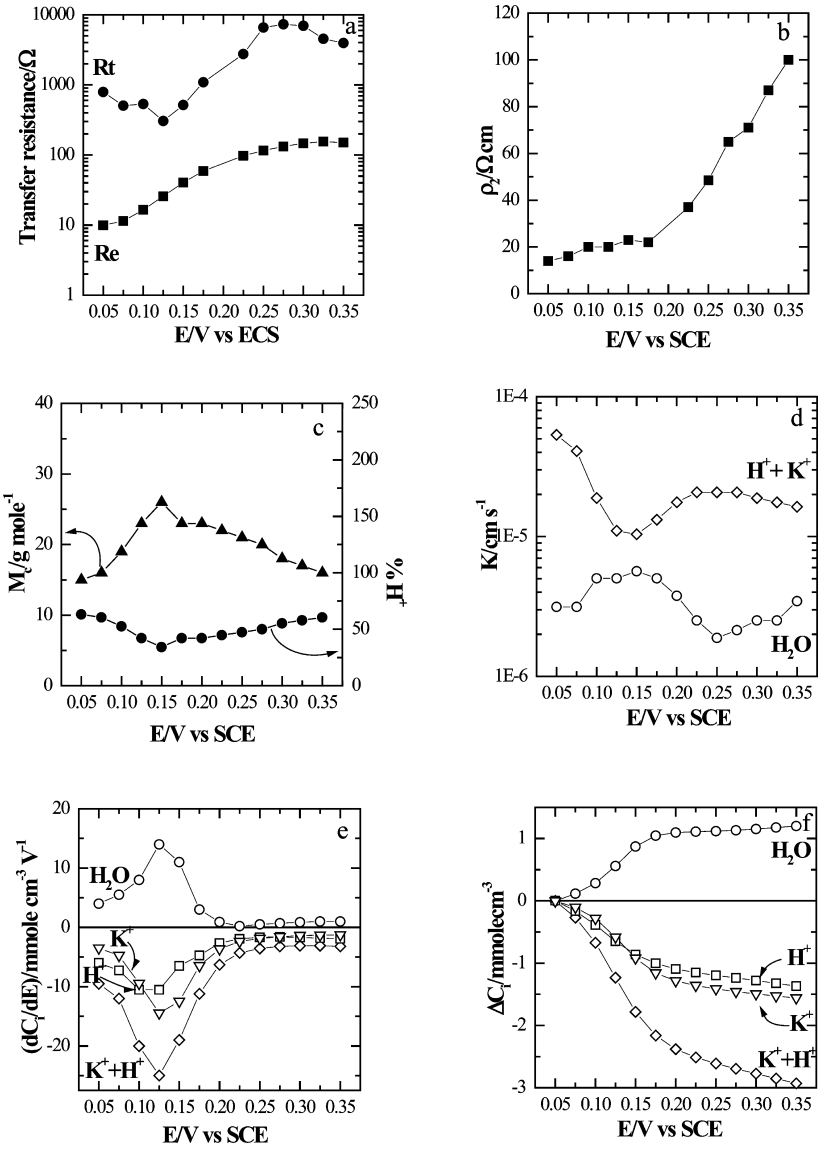

Figure 7. Variation of various calculated parameters (a–d), variation of the derivative of the insertion law (dC_i/dE) with respect to the potential (e), and variation of the species concentration (ΔC_i) with respect to the potential (f) for the PPy-HPA film in 0.1 M $KClO_4$ at pH 3.2.

about 1 g mol^{-1} for low pH, as in the 0.5 M $HClO_4$ medium, up to a few tens of grams $mole^{-1}$ for higher pH.

4.2.2. ac Electrogravimetry. ac electrogravimetric measurements were carried out on PPy-HPA films in $KClO_4$ media at pH 1.35, 3.2, and 5.2 at various potentials.

4.2.2.1. 0.1 M $KClO_4$, pH 1.35. The details of the extracted parameters are given at a potential of 0.25 V versus SCE as an example. The experimental and calculated kinetic parameters obtained by a fitting procedure for the electrochemical impedance and ac electrogravimetric data are given in Figure 5 for a measurement carried out at 0.25 V versus SCE. The diagram of the electrochemical impedance is globally similar to that of the $HClO_4$ medium, whereas the function $\Delta m/\Delta E(\omega)$ in 0.1 M $KClO_4$ at pH 1.35 shows two well-separated loops in the third and quarter quadrant of the imaginary plane, which demonstrate the exchange of at least two species in two opposite sense. The analysis of the data shows that solvent (m_s = 18 g mol^{-1}) and cations with an apparent mass (K^+ and H^+) are involved in the charge compensation process. The analysis of the data shows that solvent (m_s = 18 g mol^{-1}) and cations with an apparent mass of 4 g mol^{-1} (corresponding to 92% H^+ and 8% K^+) are involved in the charge compensation process. This apparent mass of the exchanged cations demonstrates a concomitant exchange of protons with a small number of potassium ions.

All of the calculated kinetic parameters are given in Figure 6 with respect to the potential. As for pH 0.3, the charge compensation is controlled both by electronic and ionic transfers because the resistances R_e and R_t have the same order of magnitude.

The pore resistivity is increased with the potential (Figure 6b). This could be due to the shrinking of the matrix in this potential range.

The apparent atomic mass of the involved cations changes with respect to the potential. As for $HClO_4$, it is rather constant in the left part of the graph, increases when the potential increases, and then decreases at a potential of 0.24 V. Similarly, the time constants, K_i, of the cations is larger than for the solvent (Figure 6d). This shows that the cations have exchange kinetics faster than water but exhibit minima at the peak potentials. The derivative of the insertion laws of the protons is also similar to this quantity for 0.5 M $HClO_4$ (Figure 6c). For the solvent, this

dx.doi.org/10.1021/la302115f | *Langmuir* 2012, 28, 13746–13757

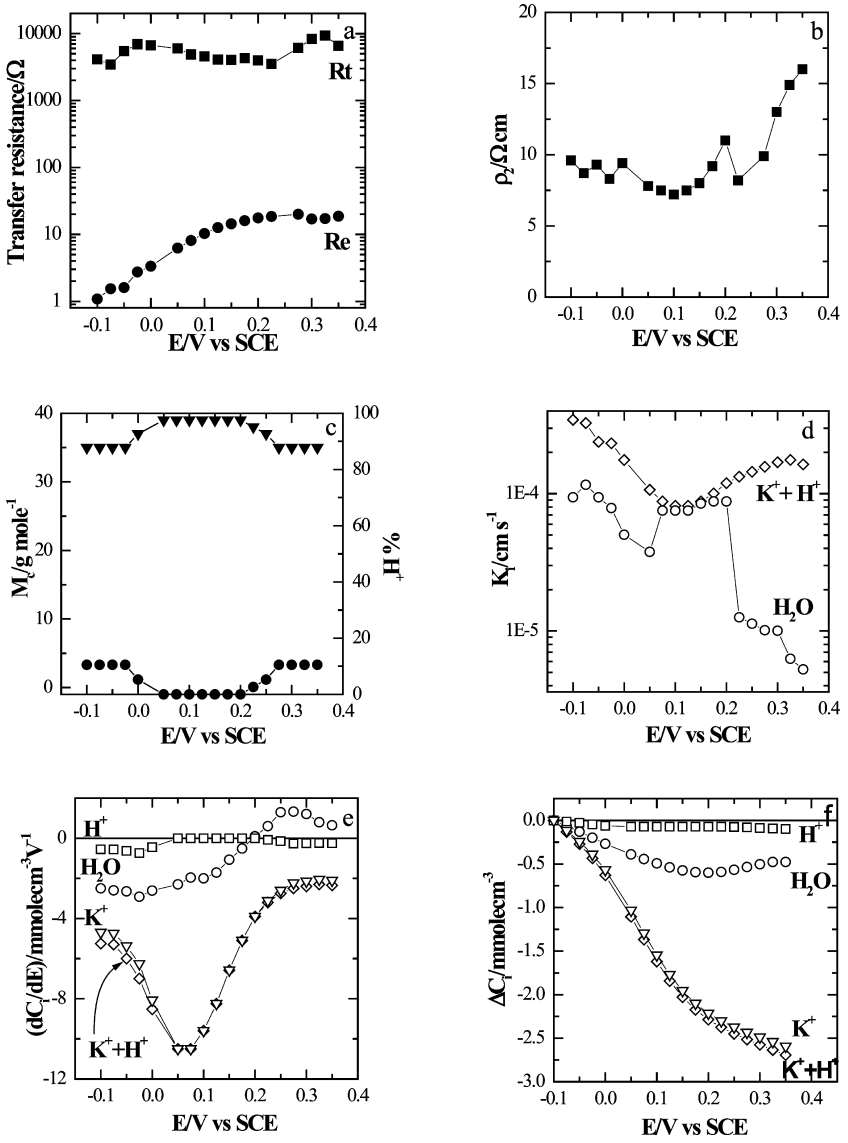

Figure 8. Variation of various calculated parameters (a–d), variation of the derivative of the insertion law (dC_i/dE) with respect to the potential (e), and variation of the species concentration (ΔC_i) with respect to the potential (f) for the PPy-HPA film in 0.1 M $KClO_4$ at pH 5.2.

quantity shows that it is exchanged in the opposite direction from the protons with an inversion at the end of the potential range of the second peak. However, contrary to the $HClO_4$ medium there is an exchange of solvent in the potential range of the first peak as well. Finally, the change in concentration, obtained by integrating the previous curves, shows that cations are expelled and water is inserted when the PPy-HPA film is oxidized in 0.5 M $KClO_4$ at pH 1.35 (Figure 6f).

4.2.2.2. 0.1 M $KClO_4$, pH 3.2. The impedance diagram has the same shape as at lower pH (Figure 5). However, the electrogravimetric transfer function shows two well-separated loops, one in the third quadrant and the other in the second quadrant of the imaginary plane, which demonstrate the exchange of at least two species but in different directions compared to that at lower pH values. The analysis of the data shows that solvent (m_s = 18 g mole^{-1}) and cations with an apparent mass (K^+ and H^+) are involved in the charge compensation process. All of the calculated kinetic parameters are given in Figure 7 with respect to the potential. Contrary to the data at lower pH values, the charge compensation is controlled only by the ionic transfer because R_e is very much smaller than R_t (Figure 7a).

As at pH 1.35, the pore resistivity is increasing with the potential (Figure 7b).

The apparent atomic mass of the involved cations increases and then decreases with respect to the potential (Figure 7c). This shows that the potassium ions are responsible for half of the positive charges exchanged during the charge compensation process. Similar to the situation at lower pH values, the time constant K_i of the cations is larger than that for the solvent (Figure 7d). This shows that the cations have exchange kinetics faster than for water. The derivatives of the insertion laws of the protons and solvent are negligible for the second redox peak (Figure 7e). In addition, it is positive for the solvent and negative for the cations, which can be separated for protons and potassium because the apparent mass of the cations is known. Therefore, for the solvent this quantity shows that it is exchanged in the opposite direction with respect to the cations. By knowing the apparent mass of the exchanged cations and the derivative of the proton insertion law, it is possible to obtain separately the derivatives of the protons and the potassium

dx.doi.org/10.1021/la302115f | *Langmuir* 2012, 28, 13746–13757

ions. Finally, the change in concentration, obtained by integrating the previous curves, shows that the two cations are expelled/inserted and water is inserted when the HPAs are oxidized/reduced in 0.5 M $KClO_4$ at pH 3.2 (Figure 7f).

4.2.2.3. 0.1 M $KClO_4$, pH 5.2. All of the kinetic parameters calculated from electrochemical impedance and electrogravimetric data are given in Figure 8 with respect to the potential. Contrary to acidic pH values, the charge compensation is totally controlled by ionic transfer because R_e is very much smaller than R_t (Figure 8a). As at pH 1.35 and 3.2, the pore resistivity increases with the potential (Figure 8b).

The apparent atomic mass of the involved cations remains close to the atomic mass of potassium (39 g mol^{-1}) whatever the potential except at the end potential where it decreases slightly, which shows some proton exchange (Figure 8c). As for other pH values, the time constant, K_i, of the cations is larger than for the solvent (Figure 8d). This shows that the cations have exchange kinetics faster than for water. The derivative of the insertion laws primarily shows the small involvement of protons in the charge compensation at pH 5.2 (Figure 8e). At this pH value, electroneutrality is mainly assured by potassium ions. Concerning water, it is expelled from or inserted into the film following the imposed potential. Finally, the change in concentration, obtained by integrating the previous curves, shows that the concentrations of the cations and water increase in the PPy-HPA film when the HPAs are reduced in 0.1 M $KClO_4$ at pH 5.2 (Figure 8f).

5. DISCUSSION

R_e does not change very much with pH, contrary to R_t, which increases very much with pH. Therefore, for the higher pH values ionic transfer is the rate-limiting step of the charge compensation process for the HPAs. However, at acidic pH values a mixed control of the redox switching is observed. At pH 0.3, the charge compensation is due to H^+ exchange (only this cation is present in the electrolyte), at pH 1.35 and 3.5, it is due to both H^+ and K^+ exchanges, and at pH 5.2 it is predominantly due to K^+. At intermediate pH values, two-electron-reduced $SiMo_{12}O_{40}^{4-}$ exists in two forms, $H_2SiMo_{12}O_{40}^{4-}$ and $HSiMo_{12}O_{40}^{5-}$, which are at almost equal concentrations (at pH 3.2, pK_{a5} = 2.9[23]). The first one corresponds to the capture of two protons (two protonation sites), and the second one corresponds to the capture of one proton (one protonation site) and the capture of one proton or one K^+ cation (nonspecific electrostatic site). This explains the preferential insertion of protons even when a large concentration of potassium ions is present in the bathing solution.

Concerning solvent, for the more acidic tested solutions, it is expelled when cations are inserted, especially in the potential range of the more cathodic peak of the voltammetric curve. For higher pH values, the role of water is opposite: it is rather going in the same direction as cations, especially for the first and second peak regions (reaction 2). The apparent discrepancy with our previous results,[9] where it was assumed that solvent is not involved, comes from the particular potentials (0.234 V vs SCE at pH 0.3, 0.164 V vs SCE at pH 3.2, and 0.114 V vs SCE at pH 5.2) investigated. It should be underlined that water contributions are very small for all pH values tested as shown in Figures 6–8.

For the electrolyte resistance, when the pH increases from 0.3 to 1.35 to 3.2 to 5.2, it varies from 1.15 to 6 to 18 and then to 19.1 Ω, which is proportional to the solution resistivity. Similarly, the apparent pore resistivity increases in a concomitant way.

Concerning the variation in the concentrations of the species involved in the charge compensation process, for the two more acidic solutions the total positive charges are practically twice the quantity observed for the two higher pH values, showing that only one electroactive site (the more cathodic) is active for more basic pH values.

6. CONCLUSIONS

In this work, the global kinetics and the exchanges of protons and free solvent at the film/electrolyte interface were investigated when a PPy film doped with HPA was polarized. The ionic and electronic transfers for the PPy-HPA system are fast because the determined values of the resistances are relatively low. Depending on the applied potential, the global kinetics is controlled by both the ionic and electronic transfers. Protons play an important role in the charge compensation whatever the imposed potential on the PPy-HPA film. These phenomena result from the acidic–basic properties of the reduced species of $SiMo_{12}O_{40}^{4-}$. A small quantity of water was also shown to be involved in the film reaction process.

AUTHOR INFORMATION

Notes

The authors declare no competing financial interest.

REFERENCES

(1) Abrantes, L. M.; Cordas, C. M.; Vieil, E. EQCM study of polypyrrole modified electrodes doped with Keggin-type heteropolyanion for cation detection. *Electrochim. Acta* **2002**, *47*, 1481–1487.

(2) Pope, M. T. *Heteropoly and Isopoly Oxometalates*; Nauka: Novosibirsk, 1990.

(3) Wang, P.; Li, Y. Electrochemical and electrocatalytic properties of polypyrrole film doped with heteropolyanions. *J. Electroanal. Chem.* **1996**, *408*, 77–81.

(4) Barth, M.; Lapkowski, M.; Lefrant, S. Electrochemical behaviour of polyaniline films doped with heteropolyanions of Keggin structure. *Electrochim. Acta* **1999**, *44*, 2117–2123.

(5) Lapkowski, M.; Bidan, G.; Fournier, M. Synthesis of polypyrrole and polythiophene in aqueous solution of Keggin-type structure heteropolyanions. *Synth. Met.* **1991**, *41*, 407–410.

(6) Cui, Y.; Wu, Q.; Mao, J. Preparation and conductivity of polypyrrole molybdotungstovanadogermanic heteropoly acid hybrid material. *Mater. Lett.* **2004**, *58*, 2354–2356.

(7) Debiemme-Chouvy, C.; Bernard, M. C.; Cachet, H.; Deslouis, C. XPS and RBS characterizations of electrosynthesized polypyrrole films doped with a heteropolyanion, $SiMo_{12}O_{40}^{4-}$. *Surf. Interface Anal.* **2006**, *38*, 531–534.

(8) Debiemme-Chouvy, C.; Cachet, H.; Deslouis, C. Investigation by EQCM of the electrosynthesis and the properties of polypyrrole films doped with sulphate ions and/or a Keggin-type heteropolyanion, $SiMo_{12}O_{40}^{4-}$. *Electrochim. Acta* **2006**, *51*, 3622–3631.

(9) Debiemme-Chouvy, C.; Rubin, A.; Perrot, H.; Deslouis, C.; Cachet, H. ac-electrogravimetry study of ionic and solvent motion in polypyrrole films doped with an heteropolyanion, $SiMo_{12}O_{40}^{4-}$. *Electrochim. Acta* **2008**, *53*, 3836–3843.

(10) de Levie, R. On porous electrodes in electrolyte solutions: I. Capacitance effects. *Electrochim. Acta* **1963**, *8*, 751.

(11) de Levie, R. On porous electrodes in electrolyte solutions–IV. *Electrochim. Acta* **1964**, *9*, 1231.

(12) de Levie, R. The influence of surface roughness of solid electrodes on electrochemical measurements. *Electrochim. Acta* **1965**, *10*, 113.

(13) Gabrielli, C.; Garcia-Jareno, J. J.; Perrot, H. Charge compensation process in polypyrrole studied by ac electrogravimetry. *Electrochim. Acta* **2001**, *46*, 4095−4103.
(14) Gabrielli, C.; Keddam, M.; Nadi, N.; Perrot, H. Ions and solvent transport across conducting polymers investigated by ac electrogravimetry. Application to polyaniline. *J. Electroanal. Chem.* **2000**, *485*, 101−113.
(15) Jackson, A.; Hillman, A. R.; Bruckenstein, S.; Jureviciute, I. *J. Electroanal. Chem.* **2002**, *524*, 90.
(16) Gabrielli, C.; Garcia-Jareno, J.; Keddam, M.; Perrot, H.; Vicente, F. ac-electrogravimetry study of electroactive thin films. I. Application to Prussian blue. *J. Phys. Chem. B* **2002**, *106*, 3182.
(17) Kim T. T. L. Ph.D. Thesis, Université Pierre et Marie Curie, Paris, 2009.
(18) Gabrielli, C.; Perrot, H. In *Modern Aspects of Electrochemistry*; Schlesinger, M., Ed.; Springer: New York, 2009; Vol. *44*, pp 151−238.
(19) Strzezik, J.; Krowiak, A.; Turek, W.; Kozie, K.; Szperlich, P. Morphology and conductivity of polymeric supportas the key factors modifying catalytic activity of Keggin type heteropolyacids dispersed in poly(N-methylpyrrole) and polypyrrole matrices. *Catal. Lett.* **2008**, *127*, 226−231.
(20) Smela, E.; Gadegaard, N. Volume change in polypyrrole studied by atomic force microscopy. *J. Phys. Chem. B* **2001**, *105*, 9395−9405.
(21) Wang, X.; Smela, E. Color and volume change in PPy(DBS). *J. Phys. Chem. C* **2009**, *113*, 359−368.
(22) Otero, T. F.; Ariza, M. J. Revisiting the electrochemical and polymeric behavior of a polypyrrole free-standing electrode in aqueous solution. *J. Phys. Chem. B* **2003**, *107*, 13954−13961.
(23) Launay, J. L.; Massart, R.; Souchay, P. Gradual reduction of molybdosilicates and related compounds. *J. Less-Common Met.* **1974**, *36*, 139−150.